Top Catal (2007) 46:349–357
DOI 10.1007/s11244-007-9006-7

ORIGINAL PAPER

A Combined Surface Science and Electrochemical Study of Tungsten Carbides as Anode Electrocatalysts

Erich C. Weigert · Michael B. Zellner · Alan L. Stottlemyer · Jingguang G. Chen

Published online: 27 November 2007

Abstract An effective anode electrocatalyst in direct methanol fuel cell (DMFC) should have high activity for the oxidation of methanol and the decomposition of water, while remaining stable under the relatively harsh anode environment. Although the Pt/Ru bimetallic alloy is currently the most effective anode electrocatalyst, both Pt and Ru are expensive due to limited supplies and both are susceptible to CO poisoning. Consequently, the discovery of less expensive and more CO tolerant alternatives to the Pt/Ru catalysts would help facilitate the commercialization of DMFC. In this paper we will discuss the possibility of using tungsten carbides (WC) and Pt-modified WC as potential anode electrocatalysts in DMFC. We will provide an overview of our recent work, using a combined approach of fundamental surface science studies and in-situ electrochemical evaluation of the activity and stability of tungsten carbides. We will demonstrate the feasibility to bridge fundamental surface science studies on single crystals with the electrochemical evaluation on polycrystalline WC films. We will also discuss the synergistic effect by supporting low coverages of Pt on the WC substrate to further enhance the electrochemical performance of WC.

Keywords Tungsten carbides · Platinum · Electrocatalyst · Fuel cells

E. C. Weigert · M. B. Zellner
Department of Materials Science and Engineering, Center for Catalytic Science and Technology (CCST), University of Delaware, Newark, DE 19716, USA

A. L. Stottlemyer · J. G. Chen (✉)
Department of Chemical Engineering, Center for Catalytic Science and Technology (CCST), University of Delaware, Newark, DE 19716, USA
e-mail: jgchen@udel.edu

1 Introduction

Recently our group has published a series of papers on surface science and electrochemical studies aimed at evaluating the feasibility of using tungsten carbides as fuel cell anode electrocatalysts for direct methanol fuel cell (DMFC) [1–8]. In this manuscript we will provide an overview of these studies, as well as some recent results on this subject. In DMFC, the anodic chemistry requires the oxidation of methanol and the decomposition of water to produce protons, electrons, and gas-phase CO_2 [9]. In addition to meeting these requirements, a desirable electrocatalyst must remain stable under the relatively harsh environment at the anode. Currently, the Pt/Ru bimetallic catalyst is the most effective anode electrocatalyst for DMFC [10–12]. Although the Pt/Ru bimetallic system exhibits desirable stability and electrochemical activity under anodic conditions, both Pt and Ru are expensive due to limited supplies. In addition, strong chemisorption of CO on Pt and Ru makes the electrocatalyst susceptible to CO poisoning, blocking the active sites for methanol oxidation. Consequently, discovery of less expensive and more CO-tolerant alternatives to the Pt/Ru catalysts would help facilitate the commercialization of DMFC.

A large body of literature exists on the possibility of using transition metal carbides to mimic the catalytic properties of Pt-group metals [13–18]. In particular, there have been many studies on tungsten carbides (WC and W_2C) since Levy and Boudart suggested that WC displayed Pt-like behavior in several catalytic reactions [19]. There have also been several attempts to utilize tungsten carbides as alternative electrocatalysts due to its stability in acidic solutions at anodic potentials [20, 21].

Our research group has investigated the activity and stability of tungsten carbides using a combination of

ultra-high vacuum (UHV) surface science studies and electrochemical measurements. These studies examined the surface reactions of methanol, water, and CO on carbide-modified W(111) and W(110) single crystal surfaces, with and without submonolayer coverages of Pt [1, 3–5, 8]. It was found that methanol readily decomposed on C/W(111) and C/W(110), although a fraction of methanol underwent a reaction pathway producing undesired gas-phase CH_4. Further investigation found that modifying the C/W(111) and C/W(110) surfaces with submonolayer coverages of Pt eliminated the reaction pathway for gas-phase CH_4, indicating a synergistic effect by supporting low coverages of Pt on the carbide surfaces. Compared to Pt, the C/W(111), C/W(110), Pt/C/W(111), and Pt/C/W(110) surfaces also showed significant increases in activity toward the dissociation of water and a reduction in the CO desorption temperatures, both of which would be very desirable for the DMFC application.

More recent studies from our group focused on bridging the materials gap between model single crystal surfaces and the more realistic, polycrystalline tungsten carbide thin film surfaces produced by physical vapor deposition (PVD) [6, 7]. Fundamental surface science techniques confirmed that the reaction pathways of methanol, water, and CO on the PVD tungsten carbides and Pt-modified tungsten carbides were similar to those on their respective single crystal surfaces [6, 7]. In addition, ex-situ cyclic voltammetry (CV) measurements indicated that phase pure WC PVD films were stable in an acidic environment when placed under typical anodic potentials. In contrast, phase pure W_2C films were not stable in the electrochemical environment, oxidizing to form surface W_xO_y species at relatively low potentials [7].

To further evaluate the activity and stability of tungsten carbides, we have recently combined electrochemical measurements with UHV techniques. An in-situ three-electrode half-cell capable of making Cyclic Voltammetry (CV) and Chronoamperometry (CA) measurements was connected via a gate valve to a UHV system equipped with X-ray Photoelectron Spectroscopy (XPS). This system allowed for surface characterization of WC and Pt-modified WC films, both before and after electrochemical measurements, without exposing the surface to air. These studies allowed us to directly compare the activity and stability of methanol oxidation over WC and Pt-modified WC films to those on pure Pt foil.

The remainder of this manuscript is organized as follows: We will first provide a brief description on the synthesis of tungsten carbide films on both single crystal surfaces and polycrystalline films. We will then discuss the surface activity of tungsten carbides toward methanol, water and CO, as well as the synergistic effect by supporting submonolayer coverages of Pt on tungsten carbides. The electrochemical studies of the activity and stability of WC and Pt/WC films will also be presented to correlate UHV surface science studies with in-situ electrochemical evaluation. Finally, we will present conclusions and future opportunities for the potential utilization of tungsten carbides as anode electrocatalysts for DMFC.

2 Experimental

2.1 Preparation of C/W(110), C/W Foil and PVD WC Films

The preparation and characterization of tungsten carbides produced on single crystal tungsten surfaces, W(111) and W(110), have been described in detail previously [15, 18]. For example, the C/W(110) surface was prepared by exposing W(110) to ethylene at 100 K and then flashed to 1,200 K. Generally these procedures were repeated for several cycles to produce a C/W(110) surface with different atomic C/W ratios. To create the WC thin films on a polycrystalline W substrate, a tungsten foil was cleaned by cycles of Ar^+ bombardment at 300 K followed by flashing to 1,200 K in vacuum. The clean W foil was carburized by decomposing ethylene using a hot filament sputter gun with 0.5 kV bias potential for 10 min. The surface was then annealed to 1,200 K to form a carbide film. X-ray photoelectron spectroscopy (XPS) analysis revealed the characteristic carbidic C 1 s feature at $\sim$282.8 eV and an atomic C/W ratio of 1.0 with no detectable impurities.

The deposition of Pt on the C/W(110) single crystal surface and the WC polycrystalline film was achieved by resistively heating a tungsten filament that was wrapped with a thin wire of 99.99+% pure Pt. After Pt deposition rate was calibrated based on the monolayer (ML) Pt coverage on the W surface, a similar deposition rate was used to form Pt-modified WC surfaces with controlled amounts of Pt, ranging from submonolayer to multilayer coverages.

2.2 Description of UHV Techniques: TPD and HREELS

Several UHV systems were used in the current study. The UHV systems are equipped with Auger electron spectroscopy (AES), XPS, low-energy electron diffraction (LEED), temperature-programmed desorption (TPD), and high-resolution electron energy loss spectroscopy (HREELS). The sample was mounted inside the UHV chamber on a differentially pumped manipulator that allowed the motion in the *X*, *Y*, and *Z* planes, as well as rotation. The W single crystal surface or polycrystalline foil was spot-welded

directly to two tantalum posts that served as electrical connections for resistive heating, as well as thermal contacts for cooling with liquid nitrogen. With this mounting scheme the temperature of the W substrate could be varied between 100 and 1,200 K.

2.3 Electrochemical Measurements: CV and CA Measurements

Electrochemical studies were performed in a three-electrode electrochemical cell composed of a platinum gauze counter electrode (99.99% purity, $\sim$15 cm^2 surface area, Alpha Aesar), a saturated calomel electrode (SCE) as the reference electrode (−0.241 V w.r.t. the normal hydrogen electrode (NHE)), and a polycrystalline metal foil, which was either tungsten carbide or platinum with $\sim$1 cm^2 surface area, as the working electrode. The electrolyte composition was of 0.05 M H_2SO_4 solution at room temperature, which was continuously pumped by peristaltic pumping at a rate of 10 mL/min from a 2 L reservoir. For the comparison of surface behavior in an environment that simulates DMFC conditions, a solution composed of 0.2 M CH_3OH in addition to 0.05 M H_2SO_4 (also at room temperature) was used. The CV measurements included the application of a potential sweep from −0.09 V to a desired potential value at a scan rate of 100 mV/s. The CA experiments involved a potential step of the working electrode surface also to a single potential value for 180 s after a 10 s delay while holding the sample at 0 V vs. open circuit potential (OCV), as described elsewhere [22].

To eliminate exposure of the sample to air during electrochemical measurements and sample transfer to and from the XPS chamber, a typical experiment proceeded as follows, similar to that developed by Goodman [23] and Stuve and Madix [24]. The WC and Pt/WC surfaces were first prepared and characterized with XPS in the UHV chamber. The sample was then positioned in the load lock chamber under vacuum and separated from the UHV chamber by closing a gate-valve. The pressure inside the load lock chamber was raised to one atmosphere using 99.999% purity N_2 and the gate valve was opened between the load lock chamber and electrochemical half-cell. At the same time, the electrochemical cell environment and liquid reservoir had been de-aerated for at least 25 min prior to filling the transfer chamber with nitrogen. At the time of adequate purging, the electrochemical cell was translated close to the sample surface to make contact between the working electrode surface and electrolyte to conduct CV or CA measurements. Immediately following the completion of electrochemical experiments, the electrochemical half-cell was retracted and isolated by closing a gate valve. The intermediate chamber was then evacuated. At sufficiently low pressures, the intermediate chamber was opened to the primary UHV chamber by another gate valve and the sample was characterized using XPS to evaluate the effects of electrochemical treatment.

3 Results and Discussion

3.1 UHV Surface Science Studies

3.1.1 TPD Results

The TPD technique is utilized to determine the reaction products of CH_3OH on tungsten carbides produced on W single crystal surfaces and polycrystalline films. For example, TPD results from 2.0 L (1 L = 10^{-6} Torr's) exposure of CH_3OH on C/W(110) and Pt-modified C/W(110) surfaces are compared in Fig. 1 [8]. Figure 1a displays molecular desorption of CH_3OH from C/W(110) and Pt-modified C/W(110) surfaces. The molecular desorption peaks of CH_3OH were relatively weak, indicating that adsorbed methanol primarily underwent decomposition instead of reversible molecular desorption.

Figure 1b, c, and d display the gas-phase desorption products from C/W(110) and Pt-modified C/W(110) surfaces. On C/W(110), the desorption of H_2 (Fig. 1b) occurred as a broad peak centered at $\sim$384 K with a shoulder at $\sim$192 K. The evolution of CH_4 (Fig. 1c) and CO (Fig. 1d) were observed at 446 and 401 K, respectively. Additional CO peaks were observed at 859 and 976 K, which were attributed to the recombinatory desorption of atomic C and O. After the surface was heated to 1,150 K, AES measurements indicated that no atomic O was present on the surface. Lastly, no detectable amounts of gas-phase formaldehyde, CO_2, or H_2O were observed from the C/W(110) surface (TPD not shown).

Similar to C/W(110), the 0.5 ML Pt/C/W(110) surface showed two H_2 desorption peaks centered at $\sim$192 and $\sim$384 K. Molecular CO desorption was detected as a relatively sharp peak at 381 K and the recombinatory CO desorption occurred as a broad peak centered at $\sim$859 K. Unlike C/W(110), the 0.5 ML Pt/C/W(110) surface did not produce any CH_4. The elimination of the CH_4 reaction pathway due to Pt-modification was similar to the effect found on Pt/C/W(111) [5].

The peak areas in the Fig. 1 can be used to quantify the decomposition pathways of CH_3OH. For example, on the C/W(110) surface, hydrogen, CO, and CH_4 were the gas-phase products, and atomic carbon and oxygen were the remaining surface species. The decomposition of CH_3OH occurs through the following pathways on C/W(110):

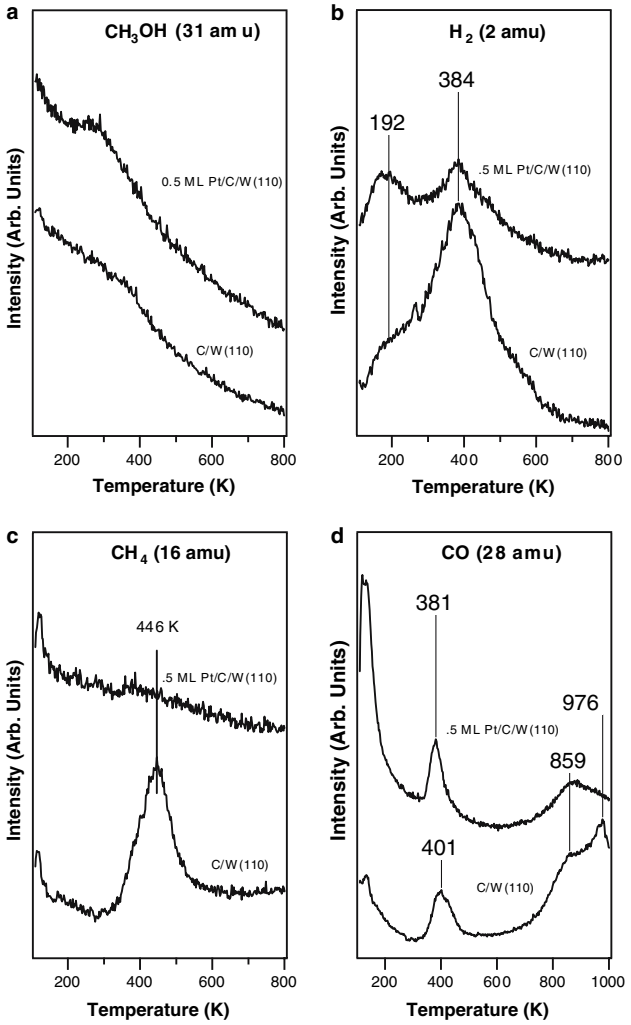

Fig. 1 TPD spectra of (**a**) CH_3OH, (**b**) H_2, (**c**) CH_4, and (**d**) H_2O following 2.0 L exposure of methanol on Pt-modified C/W(110) surfaces

$$x\mathrm{CH3OH} \xrightarrow{\Delta} x\mathrm{C(a)} + x\mathrm{O(a)} + 2x\mathrm{H2(g)} \quad (1)$$

$$y\mathrm{CH3OH} \xrightarrow{\Delta} y\mathrm{CO(g)} + 2y\mathrm{H2(g)} \quad (2)$$

$$z\mathrm{CH3OH} \xrightarrow{\Delta} z\mathrm{CH4(g)} + z\mathrm{O(a)} \quad (3)$$

Using a combination of TPD and AES, the value of x in Eq. 1, y in Eq. 2, and z in Eq. 3 have been previously determined on C/W(110) to be $x = 0.176$, $y = 0.060$, and $z = 0.068$ CH_3OH per surface W atom, respectively [8]. Table 1 summarizes the x, y, and z values for the decomposition of CH_3OH on C/W(111), Pt/C/W(111), C/W(110) and Pt/C/W(110) surfaces. The results in Table 1 indicate that all four surfaces are active toward the decomposition of CH_3OH, with the Pt-modified surfaces eliminating the undesirable pathway of CH_4 formation.

In order to bridge the materials gap and better approximate fuel cell catalyst morphology, TPD studies have been performed for the decomposition of CH_3OH on WC produced on polycrystalline W film (C/Poly W). As shown in Fig. 2, the decomposition of CH_3OH yielded gas phase hydrogen, CO, and CH_4. Hydrogen desorption was evident in a very broad peak from 270 to 800 K, likely due to the presence of different sites on the polycrystalline surfaces. The evolution of CH_4 was observed at 460 K. The desorption of CO occurred at 365 and 990 K, which were attributed to molecular desorption and the recombinatory desorption, respectively. Overall, the TPD results on polycrystalline C/W are qualitatively consistent with the decomposition on the single crystal C/W(110) surface [8].

In addition to the dissociation of CH_3OH, the effective anode catalysts for DMFC should also be active toward the dissociation of H_2O. Table 2 summarizes the dissociation activity of C/W(111) [1], 0.6 ML Pt/C/W(111) [3], C/W(110) and 0.5 ML Pt/C/W(110) [8] from TPD and AES studies. The results in Table 2 confirm that all four surfaces are active for the dissociation of H_2O.

Finally, the desorption and decomposition of CO have been investigated using TPD and AES to determine the strength of CO adsorption of on various surfaces. Table 3 summarizes the CO desorption temperatures from various surfaces. The desorption temperatures of CO from the C/W(111), Pt/C/W(111), C/W(110) and Pt/C/W(110) are significantly lower than that from Ru(0001) [25, 26] or Pt(111) [27, 28], indicating that the surface CO coverage on the carbide and Pt-modified carbide surfaces should be lower than that on Ru or Pt under typical PEMFC operating temperatures.

3.1.2 HREELS Results

Vibrational studies using HREELS have been performed to further understand the reactions of CH_3OH, H_2O and CO on the various surfaces discussed above [1–8]. For example, Fig. 3 compares the HREELS spectra following the adsorption of CH_3OH on Pt(111) and on carbide surfaces. The presence of the ν(O–H) mode at $\sim$3,300 cm^{-1} on Pt(111) indicates the molecular adsorption of CH_3OH. This is consistent with previous studies of the reaction of methanol on Pt(111) [29, 30], which reported that methanol underwent reversible adsorption/desorption under UHV conditions. The step edges and defect sites of Pt(111) lead to the decomposition of to form gas-phase H_2 and CO at temperatures >300 K. However, the overall activity toward the dissociation of methanol is rather low (1–2% of the

Table 1 Comparison of CH3OH decomposition pathways on different surfaces

Activities of C/W(111), 0.6 ML Pt/C/W(111), C/W(110), and 0.5 ML Pt/C/W(110) toward decomposition of CH_3OH				
Surface	Complete decomposition activity per W atom (%)	CO activity per W atom (%)	CH_4 activity per W atom (%)	Total no. of CH_3OH reacting per W atom
C/W(111)	0.155 (55)	0.087 (31)	0.038 (14)	0.280
0.6 ML Pt/C/W(111)	0.086 (49)	0.091 (51)	–	0.177
C/W(110)	0.176 (58)	0.060 (20)	0.068 (22)	0.304
0.5 ML Pt/C/W(110)	0.174 (78)	0.049 (22)	–	0.223

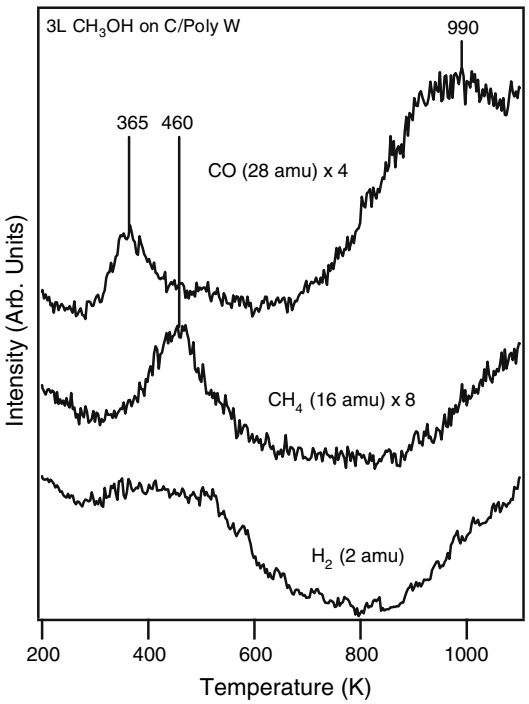

Fig. 2 TPD spectra of H_2, CH_4, and CO following 3.0 L exposure of methanol on a C/Polycrystalline W surface

Table 2 Comparison of H_2O decomposition activity on different surfaces

Activities of C/W(111), 0.6 ML Pt/C/W(111), C/W(110), and 0.5 ML Pt/C/W(110) toward decomposition of water		
Surface	Activity (water mol per W atom)	% Decomposition relative to C/W(110)
C/W(111)	0.180	118
0.6 ML Pt/C/W(111)	0.056	37
C/W(110)	0.153	100
0.5 ML Pt/C/W(110)	0.130	85

monolayer coverage) due to the low concentrations of defect sites. Furthermore, no evidence is reported that reactions of methanol on clean Pt(111) proceed through the methoxy (CH_3O) intermediate [30].

Table 3 Desorption temperature of CO from different surfaces

Desorption temperatures of CO on C/W(111), 0.3 ML Pt/C/W(111), C/W(110), 0.5 ML Pt/C/W(110), Pt(111), Ru(0001)	
Surface	Peak center of CO desorption temperature (K)
C/W(111)	330, 355
0.3 ML Pt/C/W(111)	357
C/W(111)	284, 335
0.5 ML Pt/C/W(110)	329
Pt(111)	~460
Ru(0001)	~475

In contrast, the C/W(110) surface [8] and WC polycrystalline film [7] are very active toward the dissociation of the O–H bond of CH_3OH to produce the CH_3O intermediate, as indicated by the absence of the ν(O–H) mode at ~3,300 cm^{-1}. As discussed in detail on C/W(111) [1], C/W(110) [8] and WC film [7], all the vibrational modes in Fig. 3 were related to the formation of CH_3O upon the decomposition of CH_3OH at 100 K. However, the carbide surfaces are relatively inert toward the subsequent decomposition of the methoxy species, which remain intact at temperatures up to 300 K [1, 8]. The detection of the methane product at higher temperatures, as shown in Table 1, also suggests that carbide-modified surfaces are relatively inert toward the dissociation of the C–H bonds of methoxy [1, 8].

The HREELS studies also provided insights into the synergistic effects of supporting submonolayer Pt on the carbide surfaces, which eliminates the production of the undesirable gas-phase CH_4 (Fig. 1). The origin of the observed synergistic effect can be attributed to the different chemical properties of carbide and Pt surfaces. For example, HREELS studies reveal that the methoxy intermediate is produced on the Pt/C/W(110) surfaces [8], indicating that these surfaces are, unlike Pt(111), active toward the dissociation of the O–H bond of methanol.

In addition, because Pt surfaces are very active in the cleavage of C–H bonds, the presence of Pt enhances the

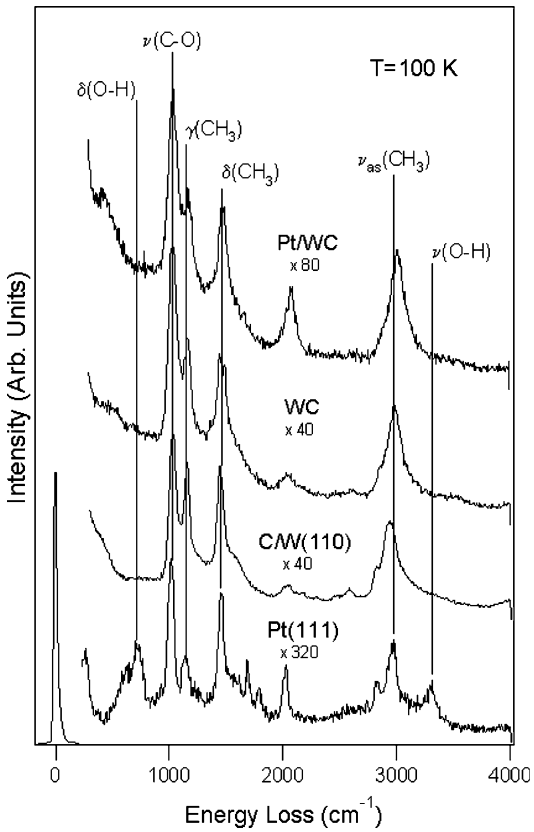

Fig. 3 HREELS results following the adsorption of CH_3OH on different surfaces at 100 K

subsequent dissociation of methoxy. Therefore, the combination of submonolayer Pt on C/W(110) leads to a unique chemistry that is not observed on either Pt or C/W(110) alone. Upon the adsorption of methanol on Pt/C/W(110), the uncovered portion of the C/W(110) surface dissociates the O–H bond of methanol to produce surface methoxy. Subsequently, the submonolayer Pt reacts with the C–H bonds of methoxy, leading to the dissociation of methoxy at temperatures that are lower than that on C/W(110) [8]. The facile C–H bond cleavage on Pt/C/W(110) should be responsible for the absence of the methane gas-phase product from the dissociation of methoxy, as confirmed in Fig. 1 and Table 1.

Overall, UHV surface science studies using TPD and HREELS indicate that tungsten carbides and Pt-modified carbides are more active than Pt(111) and Ru(0001) toward the dissociation of CH_3OH and H_2O, which are prerequisites for their potential application as the DMFC anode electrocatalysts. Equally important, these studies reveal that the desorption temperatures of CO from tungsten carbide and Pt-modified carbides are at least 100 K lower than those from either Pt(111) or Ru(0001), suggests that the carbide surfaces should be much less susceptible to CO poisoning. The challenge is to correlate the UHV surface science studies to electrochemical measurements, as described below.

3.2 Electrochemical Studies

3.2.1 Electrochemical Stability

Tungsten carbides are characterized by several phases, including WC, W_2C and WC_{1-x}. In order to determine the stability of different phases under anode conditions, we have synthesized phase pure WC and W_2C films using the PVD magnetron sputtering technique, as described previously [7]. The phase purity of the carbide films was confirmed using XRD [7]. The electrochemical stability of these two films were compared using XPS after CV measurements. For example, Fig. 4 displays the XPS results of WC and W_2C tungsten 4f peaks before and after electrochemical measurements in 0.5 M H_2SO_4. For comparison, the W 4f peak of a carbide-modified W(110) surface with an atomic ratio of C/W = $\sim$0.9 is also included. Prior to electrochemical measurements, the WC film exhibited W 4f 5/2 and 7/2 peaks at binding energies of 33.3 and 31.4 eV, respectively, which were very similar to those of the C/W(110) surface. After the CV measurement between -0.2 to 1.0 V and back to -0.2 V in a 0.5 M H_2SO_4 solution saturated with nitrogen, no significant spectroscopic changes were noticed. This observation suggests that the degree of WC oxidation is relatively minor during the CV measurement.

On the other hand, the W 4f XPS spectrum of W_2C before electrochemical measurements revealed four distinct features: carbide-modified W at 33.3 and 31.4 eV, and oxygen-modified W at 37.3 and 35.4 eV. The detection of oxygen-modified peaks was due to the oxidation of the W_2C film by air while being transferred from the PVD deposition chamber to the UHV XPS chamber. After performing electrochemical CV measurements, the W 4f peaks were completely converted to those of oxygen-modified W. The XPS results indicated that the surface regions of W_2C, within the detection limit of XPS, were completely oxidized during the CV measurements. Therefore, the CV and CA measurements in the remainder of this manuscript were performed on the relatively electrochemically stable WC phase.

In order to further evaluate the electrochemical stability of the WC phase, WC films were prepared on polycrystalline W foil and were evaluated using the in-situ half-cell. Figure 5 displays CV curves for WC and $\sim$0.8 ML Pt/WC thin film surfaces exposed to 0.05 M H_2SO_4. The samples were transferred directly from UHV to a nitrogen purged electrochemical half-cell to eliminate exposure to air. For CV measurements, the potential was referenced to the

normal hydrogen electrode (NHE) and the anodic current was defined to be negative. The working electrode (WC or Pt/WC) was cycled from −0.09 to 1.241 V and back to −0.09 V at a linear rate of 100 mV/s.

The CV curve of WC showed a cathodic current at −0.09 V due to the hydrogen evolution reaction (HER), from the recombination of H^+ ions from the sulfuric acid to form H_2 gas. Linearly increasing the potential, the WC surface displayed an anodic feature centered at ∼0.27 V, most likely resulting from the oxidation of adsorbed H that was previously generated during the HER. Further increasing the potential from ∼0.4 to ∼0.8 V resulted in no significant electrochemical activity. Beyond 0.8 V, the onset of a significant oxidation current occurred and persisted up to 1.241 V. This oxidation current is attributed to the irreversible oxidation of the WC film into W_xO_y species. As the potential of the WC working electrode was decreased, the curve retraced its path until the onset to a cathodic current at ∼0.2 V, again due to the onset of the HER [7]. In comparison, the CV curve of the 0.8 ML Pt/WC surface displayed enhanced catalyst stability in H_2SO_4. The onset voltage for oxidation increased from a value greater than 0.8 V for WC to ∼1.0 V for 0.8 ML Pt/WC. These results were confirmed from the corresponding XPS measurements before and after the CV measurements [22].

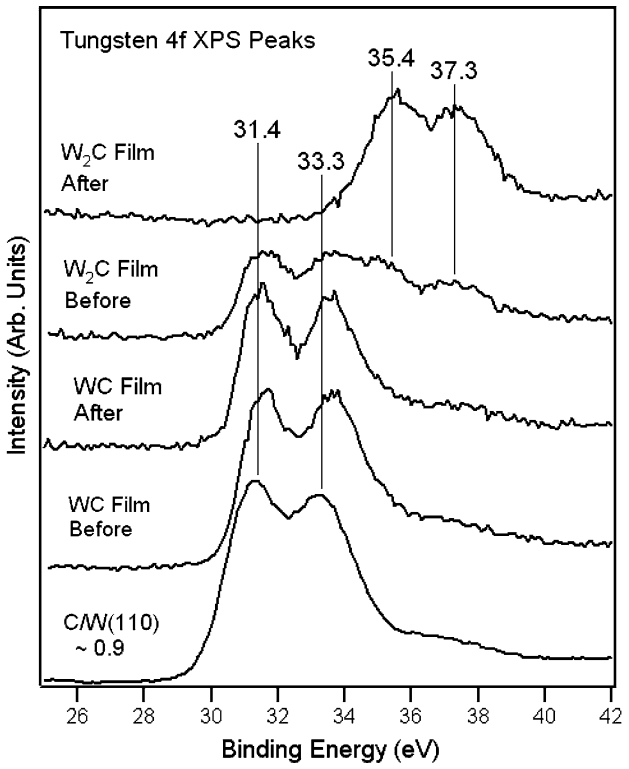

Fig. 4 W 4f WC and W_2C XPS spectra, before and after electrochemical measurements. W 4f XPS of carbide-modified W(110) with C/W ∼ 0.9 is also included

3.2.2 CV Measurements of Methanol Oxidation

The activity and stability of WC, Pt-modified WC, and Pt thin film surfaces exposed to 0.05 M H_2SO_4 with 0.2 M CH_3OH were evaluated using CV and XPS. To avoid the depletion of the methanol fuel near the electrocatalyst surface, the solution of H_2SO_4 and CH_3OH was continuously pumped from a 2 L reservoir to the electrocatalyst surface at 10 mL/min. The working electrode (WC or Pt/WC) was cycled from −0.09 to1.0 V and back to −0.09 V at a linear rate of 100 mV/s.

The CV measurements of methanol oxidation on the polycrystalline Pt foil (Fig. 6) are very similar to those in the literature [31–34]. Methanol undergoes a single oxidation state during the positive sweep of the CV cycle. The CV curve of methanol oxidation on the Pt surface shows an onset beginning at ∼0.7 V, with a maximum oxidation current of 0.2 mA/cm^2 occurring at ∼0.9 V w.r.t. NHE. The decline of this oxidation feature coincides with the onset of Pt oxidation [32–34]. The reduction of oxidation current is therefore attributed to a reduction of catalytically active sites for methanol oxidation, as discussed previously in the literature [31]. On the negative sweep of the CV curve, an increase in the current is observed with a feature centered at ∼0.7 V, resulting from surface poisoning via intermediates formed during the methanol oxidation [31].

Similar to the Pt surface, the CV curve of methanol oxidation over the WC electrocatalyst shows a single oxidation state. However, the onset of methanol oxidation occurs at a lower voltage than that on Pt, beginning at ∼0.5 V. The maximum current of ∼0.3 mA/cm^2 occurs at ∼0.65 V, just prior to the onset of WC oxidation into W_xO_y species. Unlike Pt, the negative sweep of the CV

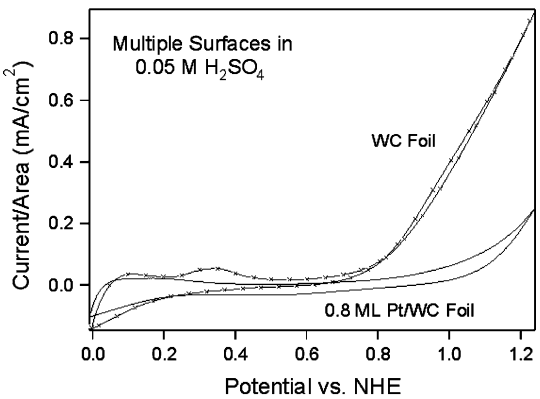

Fig. 5 CV curves of WC and monolayer Pt/WC surfaces exposed to 0.05 M H_2SO_4

curves on WC does not display any additional features. This is tentatively attributed to the weaker interactions of surface intermediates, in particular CO, with the WC and Pt-modified WC surfaces. As discussed earlier, our TPD studies of molecularly adsorbed CO on C/W single crystal surfaces have shown that the onset of CO desorption occurs at ~280 K [8], lower than the temperature regime of the CV measurements in the current study. However, the WC surface undergoes partial oxidation after repeated CV cycles, as indicated by the decrease in the oxidation current at 1.0 V from the 1st to the 30th cycle. Corresponding XPS measurements also confirm the partial oxidation of WC after multiple cycles of CV measurements [22]. The 0.8 ML Pt/WC surface shows similar methanol oxidation CV curves to those of the WC surface, with an enhancement in the stability of the electrocatalysts, as indicated by the similar CV curves from the 1st and 30th cycles. The enhanced stability is also confirmed by the corresponding XPS measurements [22].

3.2.3 CA Measurements of Methanol Oxidation

Steady-state measurements were performed using the CA technique to compare the electrochemical activity of Pt, WC, and Pt-modified WC surfaces. Results from CV studies, as described in Fig. 6, demonstrate the presence of anodic features, which result from the introduction of methanol into the electrolyte solution. Common maxima observed for these features were assigned to a potential value of ~0.65 V for both WC and Pt-modified WC surfaces.

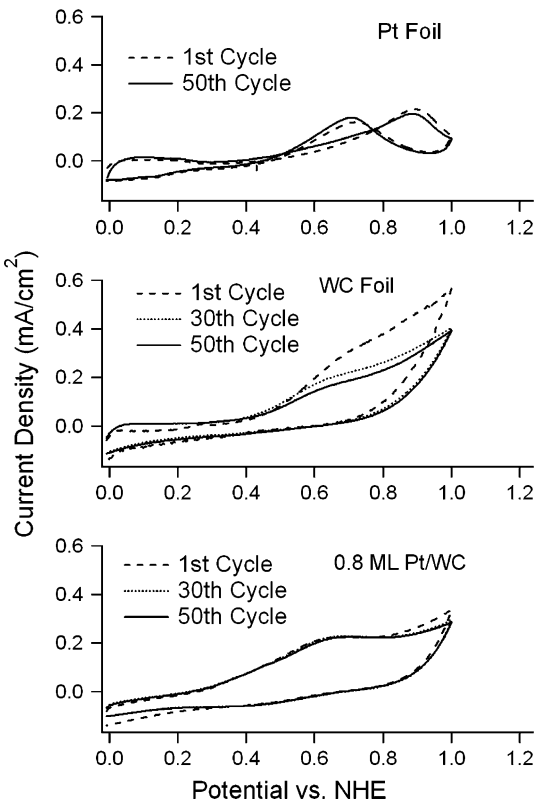

Fig. 6 CV curves of polycrystalline Pt, WC, and 0.8 ML Pt/WC surfaces exposed to 0.05 M H_2SO_4 with 0.2 M CH_3OH

Figure 7 shows the comparison of CA measurements of WC, 0.8 ML Pt/WC, and a Pt foil in a room-temperature acid and methanol solution at 0.65 V. It was found that all of the surfaces subjected to this potential achieved a steady-state Faradaic current response within 180 s of the potential step. All values of current density are normalized to the projected surface area of the specific working electrode, which was ~1 cm^2 for both the W and Pt foil working electrode surfaces.

These results suggest that there is a similar steady-state behavior for methanol oxidation between WC and 0.8 ML Pt-modified WC surfaces in a deaerated environment. In contrast, a pure Pt surface subjected to the same electrochemical potential produces a much lower current response in the presence of the acid and methanol solution. This reduction in onset potential for methanol oxidation has also been observed by Jayaraman et al. in a study of Pt-modified WO_3 surfaces in steady-state conditions [35]. In this case, the reduction in onset potential appears to result primarily from the pure WC surface. The low anodic current produced by the Pt foil suggests that the oxidation of methanol is drastically reduced within the first few seconds of the potential step because of poisoning by reaction intermediates such as chemisorbed CO.

In comparison, the WC and Pt/WC surfaces should have comparatively higher level of CO tolerance due to the lower desorption temperature of CO, as described earlier in UHV studies of CO desorption in Table 3. Thus the improved current response of the WC and Pt/WC surfaces

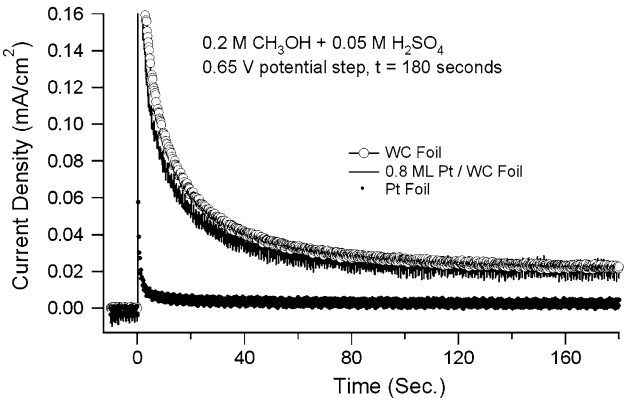

Fig. 7 CA curves of polycrystalline Pt, WC, and 0.8 ML Pt/WC surfaces exposed to a flowing 0.05 M H_2SO_4 and 0.2 M CH_3OH solution. The potentiostatic conditions are a 0.65 V potential step maintained for 180 s

is most likely due to a resistance of the surfaces to CO chemisorption in addition to a lower onset potential for methanol oxidation. Even though the WC and 0.8 ML Pt/WC surfaces show a similar steady state current in the CA measurements at 0.65 V, the presence of submonolayer Pt enhances the stability of WC, as described earlier in Fig. 6. Additional CA measurements at higher anodic potentials are underway to further evaluate the synergistic effect by supporting submonolayer Pt on WC.

4 Conclusions, Challenges, and Future Work

Based on the surface science and electrochemical results described above, the following conclusions can be made regarding the potential application of WC and Pt/WC as anode electrocatalysts in DMFC:

1. Surface science studies under UHV conditions demonstrate that the WC surfaces are more active than Pt and Ru toward the dissociation of methanol and water. In addition, the desorption temperature of CO from WC is at least 100 K lower than that from Pt or Ru, indicating higher tolerance of WC to CO poisoning under typical PEMFC operating temperatures. Furthermore, a synergistic effect is observed by depositing submonolayer coverage of Pt on WC, which eliminates the undesirable reaction pathway to produce methane.
2. Phase pure WC and W_2C films have been synthesized to correlate single crystal surfaces to polycrystalline films. Electrochemical evaluation of these thin films indicate that the W_2C phase is easily oxidized at the anode environment, while the WC phase is relatively stable at an anodic potential up to $\sim$1.0 V (NHE).
3. Electrochemical measurements using CV and CA further confirm the stability and activity of WC films for the oxidation of methanol. The combination of the in-situ half-cell and UHV system enables the evaluation of the stability of WC films before and after the CV and CA experiments. A synergistic effect is observed for supporting submonolayer Pt on WC, which enhances the electrochemical stability of WC.
4. Future work and challenges in this area include the synthesis of high surface area WC and Pt-modified WC powders that can be easily incorporated into electrode membrane assembly for full cell testing, the evaluation and improvement of the long-term stability of WC and Pt/WC at anodic potential higher than 1.0 V (NHE), and a fundamental understanding of the interfacial interaction between submonolayer Pt and the WC substrate.

Acknowledgments The authors would like to acknowledge the Department of Energy, Office of Basic Energy Sciences (Grant# DE-FG02-00ER15104) for funding of the UHV surface science studies. The synthesis and electrochemical evaluation of WC thin films are supported by the National Science Foundation (Grant # NSF/CTS 0518900).

References

1. Hwu HH, Chen JG, Kourtakis K, Lavin JG (2001) J Phys Chem B 105:10037
2. Hwu HH, Polizzotti BD, Chen JG (2001) J Phys Chem B 105:10045
3. Liu N, Kourtakis K, Figueroa JC, Chen JG (2003) J Catal 215:254
4. Hwu HH, Chen JG (2003) J Phys Chem B 107:2029
5. Hwu HH, Chen JG (2003) J Vac Sci Technol A 21:1488
6. Zellner MB, Chen JG (2004) Surf Sci 569:89
7. Zellner MB, Chen JG (2005) Catal Today 99:299
8. Zellner MB, Chen JG (2005) J Electrochem Soc 152:A1483
9. Hamnett A (1997) Catal Today 38:445
10. Parsons R, VanderNoot T (1988) J Electroanal Chem 257:9
11. Hamnett A, Kennedy BJ (1988) Electrochim Act 33:1613
12. Janssen MMP, Moolhuysen J (1976) Electrochim Act 21:869
13. Chen JG, Weisel MD, Liu Z-M, White JM (1993) J Amer Chem Soc 115:8875
14. Fruhberger B, Chen JG (1996) J Amer Chem Soc 118:11599
15. Chen JG (1996) Chem Rev 96:1477
16. Liu N, Rykov SA, Hwu HH, Buelow MT, Chen JG (2001) J Phys Chem B 105:3894
17. Polizzotti BD, Hwu HH, Chen JG (2002) Surf Sci 520:97
18. Hwu HH, Chen JG (2005) Chem Rev 105:185
19. Levy R, Boudart M (1973) Science 181:547
20. Boehm H, Pohl FA (1968) Wiss Ber AEG-Telefunken 41:46
21. Binder H, Koehlig A, Sandstede G (1969) Amer Chem Soc Div Fuel Chem Prepr 13:99
22. Weigert EC, Stottlemyer AL, Zellner MB, Chen JG (2007) J Phys Chem C (in press)
23. Goodman DW (1990) Ultramicroscopy 34:1
24. Stuve EM, Madix RJ (1985) J Phys Chem 89:105
25. de Mongeot FB, Scherer M, Gleich B, Kopatzki E, Behm RJ (1998) Surf Sci 411:249
26. Kostov KL, Rauscher H, Menzel D (1992) Surf Sci 278:62
27. Crossley A, King DA (1977) Surf Sci 68:528
28. Ertl G, Neuman M, Streit KM (1977) Surf Sci 64:393
29. Sexton BA (1981) Surf Sci 102:271
30. Gibson KD, Dubois LH (1990) Surf Sci 233:59
31. Herrero E, Franaszczuk K, Wieckowski A (1994) J Phys Chem 98:5074
32. Zelenay P, Horanyi G, Rhee CK, Wieckowski A (1991) J Electroanal Chem 300:499
33. Wieckowski A, Zelenay P, Varga KJ (1991) J Chim Phys 88:1247
34. Clavilier J, Rodes A, El Achi K, Zamakhchari MA (1991) A J Chim Phys 88:1291
35. Jayaraman S, Jaramillo TF, Baek SH, McFarland EW (2005) J Phys Chem B 109:22958